First production of pure ^{155}Gd targets and ^{155}Gd(p,x)^{155}Tb,^{156}Tb cross-section measurements

Morgane Bouteculet, Charles-Olivier Bacri, Anastasia Cassisa, Marie-Alix Duval, Alkiviadis Gourgiotis, Arnaud Guertin, Ondřej Lebeda, Jaromír Mrázek, Etienne Nigron, Eva Šimečková

Applied Radiation and Isotopes 213 (2024) 111485

Contents lists available at ScienceDirect

Applied Radiation and Isotopes

journal homepage: www.elsevier.com/locate/apradiso

First production of pure ^{155}Gd targets and ^{155}Gd(p,x)^{155}Tb, ^{156}Tb cross-section measurements

Morgane Bouteculet [a,b,*], Charles-Olivier Bacri [a,b], Anastasia Cassisa [c], Marie-Alix Duval [a,b], Alkiviadis Gourgiotis [d], Arnaud Guertin [e], Ondřej Lebeda [c], Jaromír Mrázek [c], Etienne Nigron [f], Eva Šimečková [c]

[a] Université Paris-Saclay, CNRS/IN2P3, IJCLab, 91405, Orsay, France
[b] Université Paris Cité, IJCLab, F-91405, Orsay, France
[c] Nuclear Physics Institute of the CAS, 250 68, Řež, Czech Republic
[d] Institut de Radioprotection et de Sûreté Nucléaire (IRSN), PSE-ENV/SPDR/LT2S, 92260, Fontenay-aux-Roses, France
[e] Laboratoire SUBATECH, CNRS/IN2P3, Nantes Université, IMT Atlantique, F-44307, Nantes, France
[f] GIP ARRONAX, F-44817, Saint-Herblain, France

ARTICLE INFO

Keywords:
Terbium-155
Terbium-156
Theranostic
Pure target
Proton irradiation

1. Introduction

One promising tool for internal vectorized radiotherapy is the terbium quadruplet (Müller et al., 2012; Müller et al., 2014; Formento-Cavaier et al., 2020; Dellepiane et al., 2022), which contains radio-isotopes that could be used for therapy (^{149}Tb: α therapy and ^{161}Tb: β^- therapy) as well as imaging (^{152}Tb: Positron Emission Tomography - PET - and ^{155}Tb: Single-Photon Emission Computed Tomography - SPECT -). Indeed, combinations of these isotopes represent optimal theranostic pairs as their chemistry is identical. The same bioconjugate can be then labeled with all Tb radioisotopes, forming compounds of practically same pharmacokinetic behavior for theranostics.

A major constraint is limited capability to produce these radionuclides in sufficiently large quantities and with high chemical and isotopic purity, by an economically sustainable production route (Müller et al., 2014; Duchemin et al., 2016; Favaretto et al., 2021).

The ^{155}Tb radionuclide can be formed in various nuclear reactions. Currently, the highest radionucleidic purity is achievable in spallation reactions followed by offline radioisotope separation, as performed for instance at the MEDICIS facility at CERN) (dos Santos et al., 2014) or at TRIUMF ISAC facility (Fiaccabrino D. E et al., 2021). Unfortunately, this production mode provides small activities only sufficient for pre-clinical research studies, but not potential clinical demand. In addition, the spallation reaction production requires expensive infrastructure resulting in high costs. From this point of view, cyclotron production seems to meet routine manufacturing requirements better. Among the most promising reactions are ^{155}Gd(p,n)^{155}Tb and ^{155}Gd(d,2n)^{155}Tb. However, the highest commercially available purity of ^{155}Gd (*ca* 92 %) is not sufficient for production of high purity ^{155}Tb (Dellepiane et al., 2022; Wang et al., 2023). Moreover, co-production of ^{156}Tb is unavoidable. It can notably be considered as an issue and must be taken into account due to its high energy γ rays ($E_\gamma > 1$ MeV) that increase radiation burden: ratio of equivalent dose between ^{156}Tb and ^{155}Tb can go up to ~ 10 depending of the organ (for instance, ICRP, 1994). In addition, high energy γ-rays of ^{156}Tb can also affect the SPECT image. γ rays of these ^{155}Tb and ^{156}Tb used in this experimental study are summarized in Table 1. A recent study, mainly based on calculations, on the effect of contaminants, especially ^{156}Tb, has been reported by Barbaro et al. (2024). This shows the interest of experimental data obtained with isotopically pure targets.

At IJCLab, Orsay, we have the opportunity to use a high-performance electromagnetic separator, SIDONIE (Camplan et al., 1970; Alexandre

* Corresponding author. Université Paris-Saclay, CNRS/IN2P3, IJCLab, 91405, Orsay, France.
E-mail address: morgane.bouteculet@ijclab.in2p3.fr (M. Bouteculet).

https://doi.org/10.1016/j.apradiso.2024.111485
Received 8 April 2024; Received in revised form 1 August 2024; Accepted 26 August 2024
Available online 27 August 2024

Table 1
Energy and intensities of the γ-rays of ^{155}Tb, ^{156}Tb ground state (National Nuclear Data Center (NNDC), 2024) used for quantification of ^{155}Tb, ^{156}Tb activities in this study.

	^{155}Tb $T_{½}$ = 5.32 d		^{156g}Tb $T_{½}$ = 5.34 d	
	Energy (keV)	Intensity (%)	Energy (keV)	Intensity (%)
EC decay γ rays	105.3	25.1	199.19	41
	180.1	7.5	296.49	4.5
	262.3	5.3	356.38	13.6
	340.7	1.2	422.34	8.0
			534.29	67
			925.68	3.4
			1065.11	10.8
			1154.07	10.4
			1222.44	31

et al., 1970; Chauvin et al., 2004; Bacri et al., 2017) for production of isotopically pure targets.

Here we report on the tests with first experimentally produced enriched targets of ^{155}Gd with the aim to validate the whole experimental chain from the isotope production to the final product analysis.

This work is a part of a project aiming at demonstration of the advantages of highly enriched ^{155}Gd targets for production of ^{155}Tb in the proof-of-concept phase and evaluation of the ^{156}Tb content in the product. As the two reported experiments are test experiments, not all results will be presented and we focus on ^{155}Tb and ^{156}Tb. The main goal of these test experiments was to develop and implement our methods and data analysis, and to ensure that they are trustworthy before performing a more extensive study that will cover a larger energy range relevant for the investigated evolution of production cross sections as a function of the beam energy. For these test experiments, a selection of the experimental conditions, such as beam energy, was driven by an idea to reduce the factors that would contribute to a complex situation in final products decays (energy straggling) to have a better control on uncertainties entering the development-measurement chain and the availability of beams/detectors in experienced laboratories.

Here, we report here for the first time the irradiation of 99.9% enriched ^{155}Gd targets, referred in the following as $^{pure\ 155}$Gd, for ^{155}Tb and ^{156}Tb proton-induced reactions cross section measurements. Further experiments are to be performed soon to cover a broader energy range.

Table 2
Composition of the stack used during the first irradiation (ARRONAX experiment) and proton energies at the center of each layer of the stack. All foils have been purchased from Goodfellow (UK). The $^{pure\ 155}$Gd deposit has been done with the SIDONIE separator (see §2.2).

		Purity (%)	Thickness (atoms/cm^2)	Producer	E_{center} (MeV)
^{nat}Ni		99.99	1.14 10^{20}	Goodfellow (UK)	30.5 ± 0.3
^{nat}Gd		99.0	7.55 10^{20}		29.5 ± 0.3
^{nat}Ni		99.99	1.14 10^{20}		28.5 ± 0.3
^{nat}Gd		99.0	7.55 10^{20}		27.5 ± 0.3
^{nat}Ni		99.99	1.14 10^{20}		26.4 ± 0.4
$^{pure\ 155}$Gd (target #1)	^{155}Gd deposit	99.98173 ± 0.00080	(1.050 ± 0.003) 10^{18}	home made	26.3 ± 0.4
	C backing	99.997	7.55 10^{20}	Goodfellow (UK)	

2. Materials and methods

2.1. Cross section measurements techniques

Cross section measurements were performed using the stacked-foils technique (Duchemin C. et al., 2016) followed by off-line γ-ray spectroscopy. Two irradiations were performed in order to verify the method in two independent experiments.

Our stacks were composed of ^{nat}Gd foils and enriched $^{pure\ 155}$Gd of our own production interleaved by Ni and Ti monitors dedicated to beam current verification (Tables 2 and 3). The average beam current was deduced from the total charge recorded during irradiation. It was corrected using the monitor reactions ^{nat}Ni(p,x)^{57}Ni and ^{nat}Ti(p,x)^{48}V. The fraction of the ^{57}Ni and ^{48}V activity recoiled on the following foil was carefully quantified (Červenák and Lebeda, 2020). The pure target's graphite backing (99.997%, Goodfellow) acted itself as a catcher for Gd activation products.

All the thicknesses are expressed in atoms/cm^2. For ^{nat}Gd, C backing and monitor foils, they were deduced from Goodfellow indications and weighting. For $^{pure\ 155}$Gd deposits, they were deduced from the RBS measurements that were focused on the beam spot region, (Rutherford Back Scattering, M. Mayer, 2003) and done at Orsay (see § 2.2).

The first irradiation was performed at ARRONAX, St Herblain (France) for 2 h, with a proton beam current of 121 ± 5 nA and an entrance energy of 30.7 ± 0.3 MeV. The average proton beam energy at the center of each target was calculated using stopping power range tables (Hubert et al., 1990; Northcliffe and Schilling, 1970) as a part of LISE++ software (Tarasoz and Bazin, 2008).

$^{pure\ 155}$Gd target and monitor activities were measured at Orsay two days after EOB (End Of Bombardment), while ^{nat}Gd targets were measured 11 days after EOB because of their high activities. Measurements continued for two weeks. All targets were measured multiple times by two calibrated and shielded HPGe detectors: MIRION GC4018 detector and n-type HPGe with 1.9 keV resolution at 1.33 MeV and efficiency around 18 %. The stack is described in Table 2.

The second irradiation was performed at the NPI CAS cyclotron, at Řež (Czech Republic) for 55 min, with a proton beam current of 92.4 ± 4.8 nA and an incident energy of 27.1 ± 0.2 MeV. The γ-ray spectra acquisition began 2 h after the end of the bombardment and continued for 5 days. This was impossible in the previous experiment because of the delay due to the transport. A description of the stack and the detector which was used to measure each foil or target is reported in Table 3. All detectors were shielded.

Table 3
Composition of the stack of foils in the experiment at NPI CAS, Řež, and proton energies at the center of each target. All foils have been purchased from Goodfellow (UK). The $^{pure\ 155}$Gd deposits have been done with the SIDONIE separator (see §2.2).

		Purity (%)	Thickness (atoms/cm^2)	E_{center} (MeV)	detector type
^{nat}Ti		99.6	7.32 10^{19}	27.1 ± 0.2	Coaxial HPGe Ortec GEM40P4-83-SMP
^{nat}Gd		99.0	1.96 10^{20}	26.8 ± 0.2	HPGe detector Canberra GR4520
^{nat}Ni		99.99	1.21 10^{20}	26.5 ± 0.2	Coaxial HPGe Ortec GEM40P4-83-SMP
^{nat}Ti		99.99	7.38 10^{19}	26.3 ± 0.2	Coaxial HPGe Ortec GEM40P4-83-SMP
$^{pure\ 155}$Gd (target #2)	^{155}Gd deposit	99.81980 ± 0.00136	(1.275 ± 0.003) 10^{18}	26.3 ± 0.2	HPGe Canberra GR4520
	C backing	99.997	1.25 10^{21}		
^{nat}Ti		99.6	7.38 10^{19}	25.6 ± 0.2	Coaxial HPGe Ortec GEM40P4-83-SMP
$^{pure\ 155}$Gd (target #1)	^{155}Gd deposit	99.98173 ± 0.00080	(1.050 ± 0.003) 10^{18}	25.6 ± 0.2	Planar LEGe Canberra GL0515R
	C backing	99.997	2.51 10^{21}		

During the two experiments, dead time during the measurements was kept below 5 %. The only peaks taken into account during γ-ray spectra analysis were those with the net area higher than 1000 counts.

Production cross-sections for the formation of ^{155}Tb as well as ^{156}Tb in the proton-induced nuclear reactions on ^{nat}Gd and $^{pure\ 155}$Gd were derived from γ-ray spectrometry measurements (see § 3).

2.2. Production of $^{pure\ 155}$Gd target with the SIDONIE separator at IJCLab/Orsay

SIDONIE is an electromagnetic isotopic separator built at Orsay delivering 40 keV beams of almost all stable elements up to a few mA currents. Its separation power exceeds 2000 mm × Δ M/M at the focal plane. The selected ionized isotope is slowed down to 100 eV or below to be deposited onto a backing. The separated beam is scanned both horizontally and vertically in order to make the target homogeneous.

The sample preparation necessary for isotopic analysis was performed at the LUTECE platform of the IRSN. The isotopic characterization of each target was measured by Inductively Coupled Plasma tandem Mass Spectrometry (ICP-MS/MS, Agilent 8800) of PATERSON, the IRSN's mass spectrometry platform. In order to avoid polyatomic interferences (particularly ^{155}GdH + on ^{156}Gd+) and to minimize the peak tailing (^{155}Gd + on ^{154}Gd+), the MS/MS mode with O_2 in the collision reaction cell were used and Gd+ was analyzed in GdO + ion species. Target homogeneity has been verified by the RBS measurements performed with the MOSAIC platform at Orsay (Bacri et al., 2017). The proton beam has been carefully shaped and focused so that to be incident on the homogeneous thickness target area.

Results of the isotopic analysis are reported in Table 4.

3. Data analysis and results

Activity of the radionuclides produced in the irradiated target was measured using γ-ray spectrometry. The data analysis was done using the software Fityk 1.3.1 (Wojdyr, M., 2010) and Fitzpeaks 3.71 (Fitzgerald and Servives's).

The EOB activity (A_{EOB}) of a particular radionuclide was calculated from the following equation (Červenák and Lebeda, 2020, Duchemin C. et al., 2016):

$$A_{EOB} = \frac{P_\gamma}{\varepsilon \cdot I_\gamma \cdot t_l} \frac{\lambda \cdot t_m}{(1 - e^{-\lambda t_m})} e^{\lambda t_c} \quad (1)$$

Where:

- A_{EOB} is activity of the radionuclide at the EOB (Bq)
- P_γ is net peak area of the γ line selected for the radionuclide's quantification
- λ is decay constant of the radionuclide (s^{-1})
- t_m is the real time of measurement (s)
- ε is detection efficiency at the selected γ-line energy
- I_γ is emission probability of the selected γ line (abs)
- t_l is the live time of measurement (s); $t_l = t_m$-dead time
- t_c is the cooling time, i. e. time elapsed between the EOB and start of the measurement (s)

For each studied radionuclide, its major emitted and interference-free γ-rays, reported in Table 1, were used. It permits us to verify the consistency of the deduced radionuclide activity and to present an average value. Finally, the production cross section of the radionuclide of interest is calculated (Červenák and Lebeda, 2020, Duchemin C. et al., 2016):

$$\sigma = \frac{A_{EOB}}{\varphi \cdot e \cdot \chi \cdot (1 - e^{-\lambda t_b})} \quad (2)$$

Where:

- σ is the cross section for the formation of particular radionuclide (cm^2)
- A_{EOB} is activity at the EOB for the given radionuclide (Bq), from Eq. 1
- φ is particle beam flux (s^{-1})
- e is the target thickness (atoms/cm^2)
- χ is abundance of the particular nucleus or element in the target, on which the nuclear reaction takes place. In our case, $\chi = 1$ for both ^{nat}Gd and ^{155}Gd, as we provide elemental and isotopic cross sections, respectively.
- λ is decay constant of the radionuclide produced in the nuclear reaction (s^{-1})
- t_b is the bombardment time (s)

3.1. ^{155}Tb cross section in the ^{nat}Gd (p,x) and ^{155}Gd(p,n) reaction

The obtained cross-sections for formation of ^{155}Tb in the ^{nat}Gd(p,x) nuclear reactions are presented in Fig. 1 and in Table 5.

Our measurements are in agreement with each other and also with Vermeulen's et al. (2012). The measurements also indicate production cross-sections increase for the proton energies around 30 MeV.

Measurements performed with $^{pure\ 155}$Gd targets allowed us to determine for the first time the cross sections of the ^{155}Gd(p,n)^{155}Tb reaction. Results are summarized in Table 6 and displayed in Fig. 2.

These values are significantly lower than those obtained on ^{nat}Gd, where cross sections reach 200 mb (see Fig. 2). This is due to absence of other Gd isotopes found in ^{nat}Gd that significantly contribute to the formation of ^{155}Tb in this energy region, especially the ^{157}Gd, as reported in TENDL data base (TENDL, 2023). In this case, $^{pure\ 155}$Gd naturally doesn't improve the ^{155}Tb yield, as the maximum of the ^{155}Tb cross-section from ^{155}Gd is expected at much lower energies. In addition, comparison with TENDL database (TENDL, 2023) shows that experimental values are six times lower than the predicted cross sections (see Fig. 2).

However, as shown below, the use of $^{pure\ 155}$Gd reduces remarkably the content of ^{156}Tb. This contaminant production may be an issue, especially due to its high-energy γ rays (cf. Table 1). Isotopically pure targets are usually more favorable regarding minimizing available

Table 4
Results of the isotopical analysis of the enriched targets made with SIDONIE separator. Measurements were done using the ICP-MS technique.

	Target #1 irradiated at ARRONAX and NPI CAS, Řež	Target #2 irradiated at NPI CAS, Řež
^{152}Gd/Σ(Gd) (%)	(4.3 ± 2.6) 10^{-4}	(5.5 ± 2.3) 10^{-4}
^{154}Gd/Σ(Gd) (%)	(1.25 ± 0.41) 10^{-3}	(4.32 ± 0.20) 10^{-3}
^{155}Gd/Σ(Gd) (%)	**(99.98173 ± 0.00080)**	**(99.81980 ± 0.00136)**
^{156}Gd/Σ(Gd) (%)	(5.69 ± 0.12) 10^{-3}	(1.0681 ± 0.0011) 10^{-1}
^{157}Gd/Σ(Gd) (%)	(5.33 ± 0.62) 10^{-3}	(1.996 ± 0.809) 10^{-2}
^{158}Gd/Σ(Gd) (%)	(3.93 ± 0.58) 10^{-3}	(2.695 ± 0.739) 10^{-2}
^{160}Gd/Σ(Gd) (%)	(1.64 ± 0.25) 10^{-3}	(2.216 ± 0.579) 10^{-2}

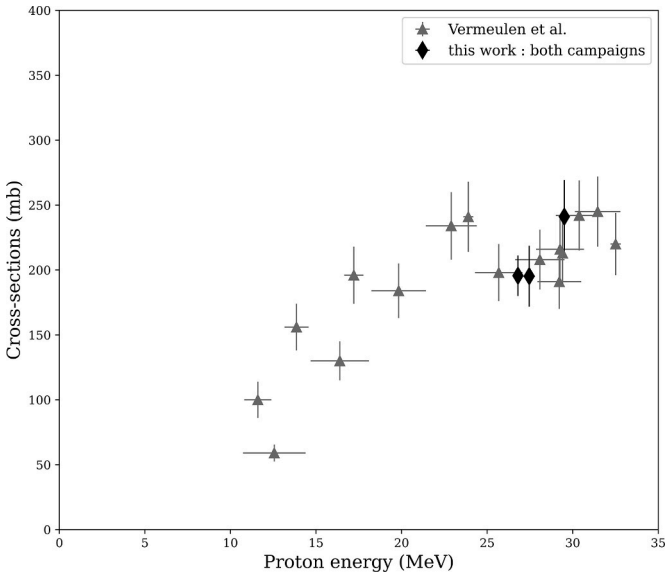

Fig. 1. ^{nat}Gd(p,x)^{155}Tb cross-section versus beam energy. Results obtained at ARRONAX and NPI CAS Řež (black diamond) compared with Vermeulen's measurements (gray triangle - Vermeulen et al., 2012).

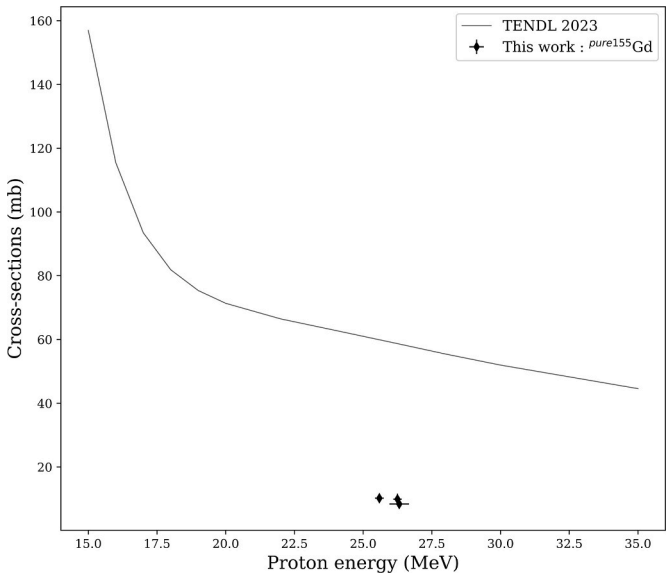

Fig. 2. ^{155}Gd(p,n)^{155}Tb versus beam energy results obtained at ARRONAX and NPI CAS Řež compared with TENDL prediction.

Table 5
Experimental cross-sections of the ^{nat}Gd(p,n)^{155}Tb reactions obtained at the ARRONAX and NPI CAS, Řež facilities.

E_p (MeV)	σ (mb) for ^{nat}Gd(p,x)^{155}Tb
29.5 ± 0.3	241 ± 28
27.5 ± 0.3	195 ± 23
26.8 ± 0.2	195 ± 16

Table 6
Obtained cross sections for the ^{155}Gd(p,n)^{155}Tb reaction at the ARRONAX and NPI CAS, Řež facilities.

E_p (MeV)	Target	σ (mb) for ^{155}Gd(p,n)^{155}Tb
26.3 ± 0.4	Target #1 *(ARRONAX irradiation)*	8.38 ± 0.76
26.3 ± 0.2	Target #2 *(NPI-CAS-Řež irradiation)*	9.89 ± 1.71
25.6 ± 0.2	Target #1 *(NPI-CAS-Řež irradiation)*	12.0 ± 1.5

reactions channels resulting in radionuclidic impurities. Since ^{156}Tb seems to be the most critical contaminant due to its impact on SPECT imaging quality and increase of the patient's radiation burden (Barbaro et al., 2024), we have also paid attention to measuring its production cross sections.

3.2. *^{156}Tb cross section in the ^{nat}Gd (p,x) and ^{155}Gd(p,γ) reactions*

^{156}Tb has three isomers: the ground state (^{156g}Tb : $T_{1/2} = 5.34$ d), the first metastable state (^{156m1}Tb, $T_{½} = 24.4$ h) and the second metastable state (^{156m2}Tb, $T_{½} = 5.4$ h). All these three are directly produced during the irradiation, while m1 and m2 states decays feed directly the ground state. Measurement of the cumulative activity of ^{156}Tb (usually labeled as ^{156cum}Tb) as a function of cooling time is of interest due to its relevance for estimating potential total ^{156}Tb activity injected to a patient. Thus, it is independent on the isomer production and feeding of the ground state. These measurements may be performed more than 60 h after the EOB, when m1 and m2 states have almost completely decayed to the ground state (see Fig. 3). The cumulative activity of the ground state is then extrapolated to the EOB using the ground state decay constant (cf. Fig. 3). However, such approach doesn't give any idea about the ^{156g}Tb activity change in time close to the EOB, as it ignores

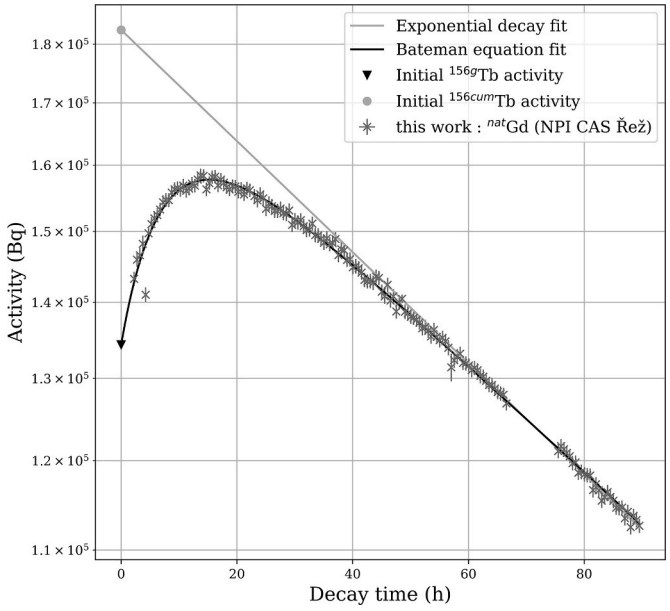

Fig. 3. Activity of ^{156g}Tb as a function of the time, where $t = 0$ correspond to t_{EOB}. Gray disc indicates cumulative activity of ^{156cum}Tb extrapolated to the EOB, while the black inversed triangle denotes actual ^{156g}Tb present at the EOB. Our experimental data on ^{nat}Gd obtained at NPI-CAS-Řež are reported as crosses. Gray line corresponds to the exponential decay constant of the ^{156g}Tb, while the black one is the result of a fit of experimental data with the Bateman equation (see Eq. (3)).

activities of the shorter-lived isomers.

Activity measurements were performed on a ^{nat}Gd target during the second irradiation campaign. Gray line corresponds to the exponential decay of the cumulative ^{156g}Tb activity extrapolated to the EOB using its half-life. Black line is a fit of the measured ^{156g}Tb activities with the Bateman equation (Eq. (3)) that include contribution of ^{156g}Tb, ^{156m1}Tb and ^{156m2}Tb in real time. The two points, gray disc and black inversed triangle at t = 0, correspond to the cumulative ^{156cum}Tb activity extrapolated to the EOB and ^{156g}Tb activity itself extrapolated to the EOB from the Bateman equation fit, respectively.

Deconvolution of this decay curve is possible using the Bateman

Table 7
Independent reaction cross sections for the ^{nat}Gd(p,x)^{156g,156m1,156m2}Tb obtained from fitting the data measured at the NPI, Řež facility for $E_p = 27.1$ MeV.

Production cross-section from ^{nat}Gd (mb)			
Direct measurement	Deduced from Bateman equation fit		
^{156cum}Tb	^{156m1}Tb	^{156m2}Tb	^{156g}Tb
337. ± 18.	15.7 ± 0.9	112. ± 6.	220. ± 12.

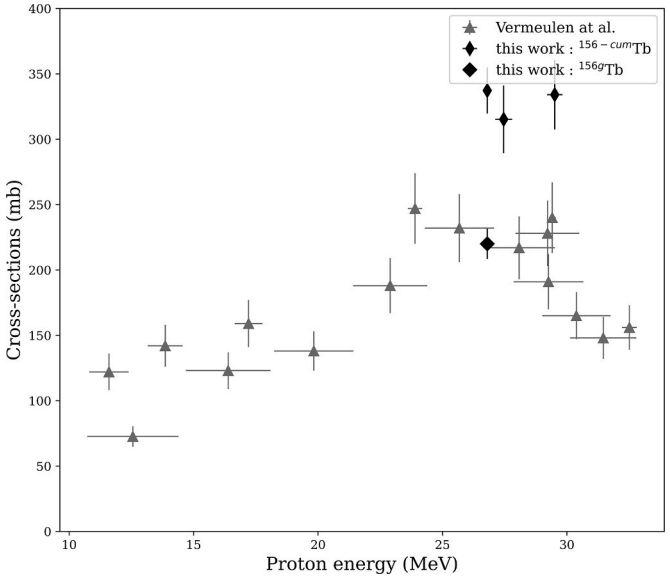

Fig. 4. ^{nat}Gd(p,x)^{156}Tb cross-section versus proton beam energy. Small diamonds (our work), triangles (Vermeulen et al., 2012) and squares (Dellepiane et al., 2022) represent ^{156cum}Tb cross-section. Large diamond corresponds to ^{156g}Tb activity deduced from applying the Bateman equation on the measurement performed in NPI CAS, Řež.

Table 8
Obtained cross sections for the ^{155}Gd(p,γ)^{156cum}Tb reaction at the ARRONAX and NPI CAS, Řež facilities.

E_p (MeV)	Target	σ (mb) for ^{155}Gd(p,γ)^{156cum}Tb
26.3 ± 0.4	Target #1 *(ARRONAX irradiation)*	0.66 ± 0.16
26.3 ± 0.2	Target #2 *(NPI-CAS-Řež irradiation)*	0.65 ± 0.11
25.6 ± 0.2	Target #1 *(NPI-CAS-Řež irradiation)*	No signal

equation for this particular case (Dellepiane et al., 2022):

$$A_{cum}(t) = A_g(0)e^{-\lambda_g t} + \frac{\lambda_g}{\lambda_g - \lambda_{m1}}A_{m1}(0)\left[e^{-\lambda_{m1}t} - e^{-\lambda_g t}\right] + \frac{\lambda_g}{\lambda_g - \lambda_{m2}}A_{m2}(0)\left[e^{-\lambda_{m2}t} - e^{-\lambda_g t}\right] \quad (3)$$

Where $A_g(0)$, $A_{m1}(0)$ and $A_{m2}(0)$ are respectively the EOB activities of ^{156g}Tb, ^{156m1}Tb and ^{156m2}Tb, and λ_g, λ_{m1} and λ_{m2} respectively their decay constants.

The activities of the isomers, $A_g(0)$, $A_{m1}(0)$ and $A_{m2}(0)$ necessary for their independent cross section calculation were deduced from the fit of this Bateman equation onto our measurements. Moreover, we have also calculated the cumulative cross-section of ^{156}Tb using the previously described usual method. The obtained results are summarized in Table 7.

These results were be compared in Fig. 4 with those reported by Vermeulen (Vermeulen et al., 2012).

Even if the results from our two experiments are compatible with each other, our ^{156cum}Tb measurements are not compatible with Vermeulen's et al. (2012) measurements that are for 30% smaller. Surprisingly, our cross section for direct formation of ^{156g}Tb seems to agree well with the cumulative cross-sections for this ground state reported by Vermeulen's et al. (2012).

Such discrepancy deserves clarification. However, one can also note that there is a difference of a similar magnitude between Dellepiane's and Vermeulen's measurements at lower energies. We hope that further measurements at various energies will help to solve this inconsistency.

Additionally, measurements performed with ^{pure} ^{155}Gd targets only allowed us to obtain the cumulative cross-sections of ^{156cum}Tb, as activity of ^{156g}Tb was too low to follow its decay.

These results reported in Table 8 show that the production of ^{156cum}Tb with ^{pure} ^{155}Gd targets is significantly lower than with ^{nat}Gd targets in the 25–30 MeV range. Although this energy range is not the most interesting for production of ^{155}Tb, it confirms very low production rate of ^{156}Tb. Further measurements in an energy range covering relevant cross-sections region are needed to identify the optimal proton energy for production of ^{155}Tb with the lowest production of ^{156}Tb.

3.3. ^{156}Tb/^{155}Tb production cross-section ratios

In order to compare production of ^{155}Tb and ^{156}Tb impurity content in different targets, we have calculated the production cross-section ratio of ^{156cum}Tb and ^{155}Tb for both ^{nat}Gd and ^{pure} ^{155}Gd targets. Results are summarized in Table 9.

The cross-section ratio $\frac{\sigma(^{155}Tb)}{\sigma(^{156cum}Tb)}$ is higher by about an order of magnitude for ^{pure} ^{155}Gd targets compared to the ^{nat}Gd targets. ^{pure} ^{155}Gd targets are obviously much more favorable for production of ^{155}Tb with minimized ^{156}Tb content using proton activation.

Table 9
The cross-section ratio $\frac{\sigma(^{155}Tb)}{\sigma(^{156cum}Tb)}$ for the two ^{nat}Gd and ^{pure} ^{155}Gd targets measured at ARRONAX and NPI CAS, Řež. The target #1 measurement results from the ARRONAX irradiation campaign.

$\frac{\sigma(^{155}\text{Tb})}{\sigma(^{156cum}\text{Tb})}$				
E_p (MeV)	^{nat}Gd target (this work)	^{nat}Gd target with ^{156cum}Tb fromVermeulen et al.	$\frac{\sigma(^{155}\text{Tb})}{\sigma(^{156cum}\text{Tb})}$	
29.5 ± 0.3	0.6 ± 0.1	0.8 ± 0.1	E_p (MeV)	^{pure} ^{155}Gd target (#1)
27.5 ± 0.3	0.7 ± 0.1	0.9 ± 0.1	26.3 ± 0.4	14. ± 5.
26.8 ± 0.2	0.6 ± 0.1	0.9 ± 0.1	26.3 ± 0.2	15 ± 4

4. Conclusions/perspectives

For the first time, ^{155}Gd targets with an enrichment larger than 99.8 % have been prepared and irradiated with protons in two independent test experiments.

Cross sections of the ^{nat}Gd(p,x)^{155}Tb and ^{nat}Gd(p,x)^{156}Tb nuclear reaction in the energy range of 25–30 MeV have been measured to verify the robustness of our measurements, and ^{155}Gd(p,n)^{155}Tb and ^{155}Gd(p,γ)^{156}Tb have been investigated.

Concerning the ^{155}Tb production with ^{nat}Gd target, our results are in agreement with measurements published by Vermeulen's et al. (2012). Moreover, as ^{156}Tb is a critical contaminant that cannot be avoided in the cyclotron production route, its formation was also investigated. Proper evaluation of ^{156g}Tb production is challenging due to formation of its two metastable states. Our ^{156cum}Tb measurements are not compatible with Vermeulen's et al. (2012). Further measurements are necessary in order to identify the source of the discrepancy.

Our measurements of the ^{155}Gd(p,n)^{155}Tb reaction shows clearly that prediction of the TALYS nuclear reaction model code adopted from the TENDL library overestimates our results *ca* six times.

In the 25–30 MeV energy range, cross-section ratio $\frac{\sigma(^{155}Tb)}{\sigma(^{156cum}Tb)}$ revealed superiority of ^{pure} ^{155}Gd over ^{nat}Gd regarding ^{156}Tb content in ^{155}Tb.

Further experiments covering the cross sections of the proton-induced nuclear reactions on ^{pure} ^{155}Gd in the proton energy range of 9–25 MeV are to be performed soon in order to find optimal ^{155}Tb production conditions. Optimum (proton energy, target thickness and purity, etc.) will be a compromise between a high production rate of ^{155}Tb and a low production rate of contaminants.

CRediT authorship contribution statement

Morgane Bouteculet: Writing – review & editing, Writing – original draft, Visualization, Investigation, Formal analysis. **Charles-Olivier Bacri:** Writing – review & editing, Whole supervision, Project administration, Investigation, Funding acquisition. **Anastasia Cassisa:** Investigation (NPI-Řež experiment). **Marie-Alix Duval:** Writing – review & editing, Investigation. **Alkiviadis Gourgiotis:** Writing – review & editing, Investigation, Formal analysis. **Arnaud Guertin:** Writing – review & editing, Investigation (ARRONAX experiment). **Ondřej Lebeda:** Writing – review & editing, Resources, Investigation, Formal analysis (NPI-Řež experiment). **Jaromír Mrázek:** Writing – review & editing, Resources, Investigation, Formal analysis (NPI-Řež experiment). **Etienne Nigron:** Writing – review & editing, Investigation (ARRONAX experiment). **Eva Šimečková:** Investigation (NPI-Řež experiment).

Declaration of competing interest

Authors declare that there is no competing interest.

Data availability

Data will be made available on request.

Acknowledgements

This research has been partially funded by the TTRIP project (2022–2025) of the French National Research Agency (ANR) under the project ANR-21-CE19-0037-01. Financial support has also been obtained through a grant from the MITI (Mission for Transversal and Interdisciplinary Initiatives) of CNRS, the French National Centre for Scientific Research.

The NPI Řež - experiment was carried out at the CANAM infrastructure. It was supported by the French-Czech project SPIRAL2-CZ EF16_013/0001679 and the NuAG (Nuclear Astrophysics and radiobioloGy) bilateral agreement between NPI and GANIL/SPIRAL2.

Isotopic measurements of the targets were done at PATERSON, the IRSN's mass spectrometry platform, under the contribution number 25.

IJCLab team wants to thank all the SIDONIE exploitation team for the fabrication of the enriched targets, and H. Lefort from IJCLab, for his technical work during the preparation of experiments.

References

Alexandre, K., Camplan, J., Ligonniere, M., Meunier, R., Sarrouy, J.L., Smith, H.J., Vassent, B., 1970. SIDONIE, the new electromagnetic isotope separator at Orsay; part II: performances. Nucl. Instrum. Methods 84, 45–54.

Bacri, C.O., Bachelet, C., Baumier, C., Bourçois, J., Delbecq, L., Ledu, D., Pauwels, N., Picard, S., Renouf, S., Tanguy, C., 2017. SCALP, a platform dedicated to material modifications and characterization under ion beam. Nucl. Instrum. Methods Phys. Res. B 406, 48–52. https://doi.org/10.1016/j.nimb.2017.03.036. https://mosaic.ijclab.in2p3.fr/en/home/.

Barbaro, F., Luciano, C., Uzunov, N., De Nardo, L., Mendelez-Alafort, L., 2024. ^{155}Tb production cross section by cyclotrons: what level of ^{155}Gd enrichment allows clinical applications? EJNMMI Physics 11, 26. https://doi.org/10.1186/s40658-024-00630-6.

Camplan, J., Meunier, R., Sarrouy, J.L., 1970. SIDONIE, the new electromagnetic isotope separator at Orsay; part I: design and construction. Nucl. Instrum. Methods 84, 37–44.

Červenák, J., Lebeda, O., 2020. New cross-section data for proton-induced reactions on ^{nat}Ti and ^{nat}Cu with special regard to the beam monitoring. Nucl. Instrum. Methods Phys. Res. B 480, 78–97. https://doi.org/10.1016/j.nimb.2020.08.006.

Chauvin, N., Dayras, F., Le Du, D., Meunier, R., 2004. SIDONIE: an electromagnetic isotope separator for preparation of high purity thin targets. Nucl. Instrum. Methods A521, 149. https://doi.org/10.1016/j.nima.2003.11.417.

Dellepiane, G., Casolaro, P., Favaretto, C.V., Grundler, P., Mateu, I., Scampoli, P., Talip, Z., Van der Meulen, N.P., Braccini, S., 2022. Cross section measurement of terbium radioisotopes for an optimized ^{155}Tb production with an 18 MeV medical PET cyclotron. Appl. Radiat. Isot. 184, 110175 https://doi.org/10.1016/j.apradiso.2022.110175.

Duchemin, C., Guertin, A., Haddad, F., Michel, N., Métivier, V., 2016. Deuteron induced Tb-155 production, a theranostic isotope for SPECT imaging and auger therapy. Appl. Radiat. Isot. 118, 281–289. https://doi.org/10.1016/j.apradiso.2016.09.030.

Favaretto, C., Talip, Z., Borgna, F., Grundler, P.V., Dellepiane, G., Sommerhalder, A., Schibli, R., Braccini, S., Müller, C., Van der Meulen, N.P., 2021. Cyclotron production and radiochemical purification of terbium-155 for SPECT imaging EJNMMI radiopharm. Chem 6, 37.

Fiaccabrino, D.E., Kunz, P., Radchenko, V., 2021. Potential for production of medical radionuclides with on- line isotope separation at the ISAC facility at TRIUMF and particular discussion of the examples of 165Er and 155Tb. Nucl. Med. Biol. 94–95, 81–91. https://doi.org/10.1016/j.nucmedbio.2021.01.003.

Fitzgerald J, Servives's JC. Software Fitzpeaks Gamma Analysis Software, Software version 3.66. Oxfordshire, http://www.jim-fitz.com/fitzpeak.htm.Last access 2024, June, the 25th.

Formento-Cavaier, R., Haddad, F., Alliot, C., Sounalet, T., Zahi, I., 2020. New excitation functions for proton induced reactions on natural gadolinium up to 70 MeV with focus on 149Tb production. Nucl. Instrum. Methods Phys. Res. Sect. B Beam Interact. Mater. Atoms 478, 174–181. https://doi.org/10.1016/j.nimb.2020.06.029.

Hubert, F., Bimbot, R., Gauvin, H., 1990. Range and stopping-power tables for 2.5–500 MeV/nucleon heavy ions in solids, Atom. Dat. and Nucl. Dat. Tabl. 46, 1–213. https://doi.org/10.1016/0092-640X(90)90001-Z.

Manuel dos Santos Augusto, R., et al., 2014. CERN-MEDICIS (medical isotopes collected from ISOLDE): a new facility. Appl. Sci. 4, 265–281.

Mayer, M., 2003. Rutherford Backscattering Spectrometry (RBS), Workshop on Nuclear Data for Science and Technology: Materials Analysis, pp. 19–30. Trieste.

Müller, C., Fischer, E., Behe, M., Köster, U., Dorrer, H., Reber, J., Haller, S., Cohrs, S., Blanc, A., Grünberg, J., Bunka, M., Zhernosekov, K., Van der Meulen, N.P., Johnston, K., Türler, A., Schibli, R., 2014. Future prospects for SPECT imaging using the radiolanthanide terbium-155 - production and preclinical evaluation in tumor-bearing mice. Nucl. Med. Biol. 41 (Suppl. l), e58–e65. https://doi.org/10.1016/j.nucmedbio.2013.11.002. Epub 2013 Nov 15. PMID: 24360901.

National Nuclear Data Center (NNDC), 2024. Decay radiation. extracted from. https://www-nds.iaea.org/relnsd/vcharthtml/VChartHTML.html. Last access: 2024, January the 23th.

Müller, C., Zhernosekov, K., Köster, U., Johnston, K., Dorrer, H., Hohn, A., van der Walt, N., Türler, A., Schibli, R., 2012. A unique matched quadruplet of terbium radioisotopes for PET and SPECT and for α- and β^--radionuclide therapy: an in vivo proof-of-concept study with a new receptor-targeted folate derivative. J. Nucl. Med. 53, 1951–1959. https://doi.org/10.2967/jnumed.112.107540.

Northcliffe, L.C., Schilling, R.F., 1970. Range and stopping-power tables for heavy ions. Nucl. Data Tables A7, 233. https://doi.org/10.1016/S0092-640X(70)80016-X.

Tarasoz, O.B., Bazin, D., 2008. LISE++: radioactive beam production with in-flight separators. Nucl. Instrum. Methods Phys. Res. B 266, 4657–4664. https://doi.org/10.1016/j.nimb.2008.05.110.

TENDL, TALYS-based evaluated nuclear data library Data extracted from https://tendl.web.psi.ch/tendl_2023/tendl2023.html Last access 2024, March, the 1st.

Vermeulen, C., Steyn, G.F., Szelecsényi, F., Kovács, Z., Suzuki, K., Nagatsu, K., Hohn, A., Van der Walt, T.N., 2012. Cross sections of proton-induced reactions on natGd with special emphasis on the production possibilities of 152Tb and 155Tb. Nucl. Instrum. Methods B 275, 24–32. https://doi.org/10.1016/j.nimb.2011.12.064.

Wang, Y., Sounalet, T., Guertin, A., Nigron, E., Michel, N., Haddad, F., 2023. Study of terbium production from enriched Gd targets via the reaction ^{155}Gd(d,2n)^{155}Tb. Appl. Radiat. Isot. 201, 110996 https://doi.org/10.1016/j.apradiso.2022.110287.

Wojdyr, M., 2010. *Fityk*: a general-purpose peak fitting program. J. Appl. Crystallogr. 43, 1126–1128.